ACS APPLIED MATERIALS & INTERFACES

Research Article

www.acsami.org

Pillar[6]arene-Valved Mesoporous Silica Nanovehicles for Multiresponsive Controlled Release

Xuan Huang and Xuezhong Du*

Key Laboratory of Mesoscopic Chemistry (Ministry of Education), State Key Laboratory of Coordination Chemistry, and School of Chemistry and Chemical Engineering, Nanjing University, Nanjing, Jiangsu 210093, People's Republic of China

Supporting Information

ABSTRACT: The synthesis and host–guest chemistry of pillararene (PA) derivatives are a hot research topic, and the applications of PAs in relevant research fields are essential to explore. Carboxylate-substituted pillar[6]arene (CPA[6])-valved mesoporous silica nanoparticles (MSNs) functionalized with dimethylbenzimidazolium (DMBI) and bipyridinium (BP) stalks were constructed, respectively, for multiresponsive controlled release. CPA[6] encircled the DMBI or BP stalks to develop supramolecular nanovalves for encapsulation of cargo within the MSN pores. The release of cargo was triggered by acidic pH or competitive binding for the dethreading of CPA[6] and the opening of the nanovalves; moreover, coordination chemistry is the first strategy to activate CPA nanovalves by metal chelating with the carboxylate groups of CPA for cargo release. The controlled release of the CPA[6]-valved MSN delivery systems can meet diverse requirements and has promising biological applications in targeted drug therapy.

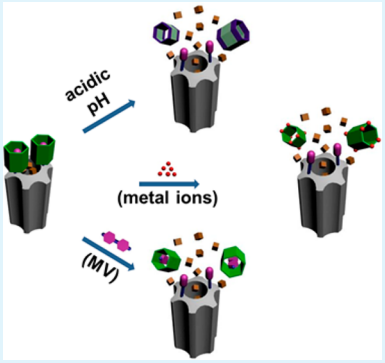

KEYWORDS: *controlled release, drug delivery, mesoporous silica nanoparticle, nanovalve, pillararene*

INTRODUCTION

Stimuli-responsive drug delivery systems are highly desirable in clinical medicine concerning enhanced therapeutic efficacy and minimized adverse effects of drugs.[1] In comparison with polymeric nanoparticles, micelles, and liposomes, mesoporous silica nanoparticles (MSNs) have emerged as an ideal drug container owing to high surface area, large pore volume, uniform and tunable pore size, good biocompatibility, and easy and diverse functionalization.[2−6] Much attention has been focused on mechanized MSNs integrated with nanovalves, capable of regulating controlled release of trapped cargo in the MSN pores. Nanovalves are machines constructed from a moving part, which consists of a macrocyclic host that slides along a thread-like molecule between one or more binding stations.[7] The movable ring acts as a valve to control the access of cargo to and from the MSN pores. The MSN vehicles capped with supramolecular nanovalves have been extensively studied, in which cyclodextrins,[8−13] calixarenes,[14,15] and cucurbiturils[16−24] encircled the thread-like molecules immobilized on the MSN surface. The nanovalves can be activated for controlled release with a variety of stimuli, such as pH,[8,13,16−18,20,23,24] redox,[13,19] light,[15,22] enzyme,[10,11,14,21] and competitive binding[20,21] in aqueous solutions.

Pillararenes (PAs), a new type of synthetic macrocyclic hosts, are paracyclophane derivatives consisting of 1,4-disubstituted hydroquinone units linked by methylene bridges in their 2,5 positions.[25] The synthesis and host–guest chemistry of pillararene (PA) derivatives in solutions are a hot research topic,[26−30] and it is essential to explore the applications of PAs in relevant research fields. Recently, water-soluble carboxylate-substituted pillar[5]arene (CPA[5]) was used to construct mechanized MSNs as a nanovalve for controlled release.[31] Carboxylate-substituted pillar[6]arene (CPA[6]) with a cavity of relatively big size was first synthesized in 2012[32] and can include a variety of guest molecules of interest with a high binding affinity in principle. However, only two guests have been so far reported to have a high binding affinity for CPA[6]. One is 1,1′-dimethyl-4,4′-bipyridinium (methyl viologen, MV), which formed a 1:1 inclusion complex with CPA[6] with the association constant of $(1.02 \pm 0.10) \times 10^8$ M^{-1},[33] and the other is ferrocenium methanamine, which formed a 1:1 inclusion complex with CPA[6] with the association constant of $(1.27 \pm 0.42) \times 10^5$ M^{-1}.[34]

Herein, a new guest, 1,3-dimethyl-2-methylmercaptobenzimidazolium (DMBI-SM), was synthesized and could form a 1:1 inclusion complex with CPA[6] with a high binding affinity; furthermore, the CPA[6] supramolecular nanovalves based on MSN vehicles functionalized with dimethylbenzimidazolium (DMBI) or bipyridinium (BP) as stalks were constructed for multiresponsive controlled release (Scheme 1). In acidic solutions, pH-responsive controlled release could be realized because CPA[6] was protonated to be insoluble and dethreaded from the functionalized stalks. CPA[6] has 6 carboxylate groups at each end and could be chelated by divalent metal ions in neutral aqueous solutions. Metal chelating-triggered controlled release was reported for the

Received: September 3, 2014
Accepted: October 22, 2014
Published: October 22, 2014

Scheme 1. Illustration of CPA[6]-Valved MSN Vehicles Functionalized with DMBI or BP Stalks for Multiresponsive Controlled Release Triggered by Acidic pH, Metal Chelating, and Competitive Binding

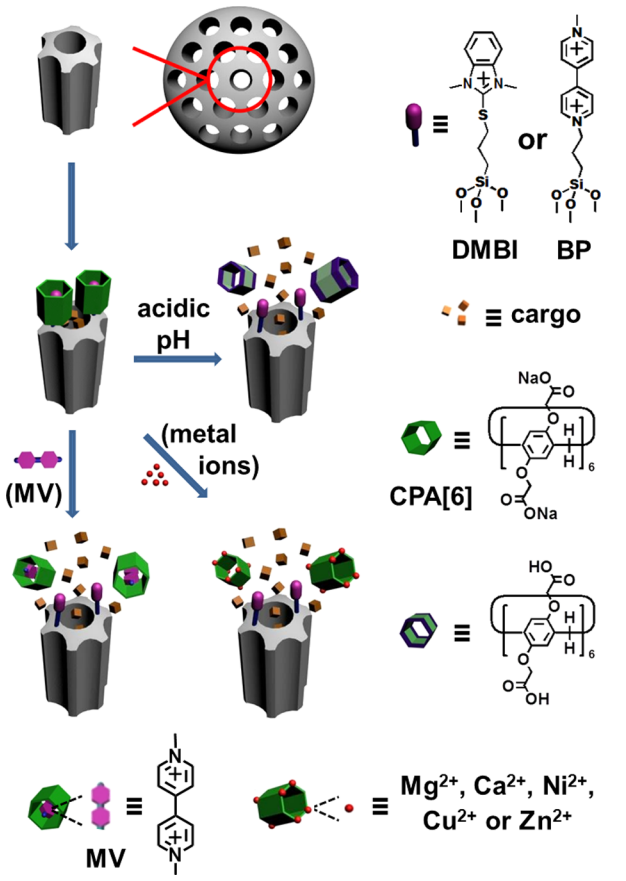

first time for CPA nanovalves. In addition, the supramolecular nanovalves could be activated by competitive binding of MV for controlled release. It is clear that the CPA[6]-valved MSN vehicles have promising biological applications in targeted drug therapy.

EXPERIMENTAL SECTION

Materials. CPA[6] was synthesized according to the method reported recently[32] with a little modification (Supporting Information, Chart S1 and Figures S1−S8); DMBI-SM (Supporting Information, Chart S2 and Figures S9 and S10) and BP-derived propyltriethoxysilane (BP-PTS) (Supporting Information, Chart S3 and Figures S11−S16) were synthesized in our laboratory, and MV was synthesized according to the literature (Supporting Information, Figures S17 and S18).[35] Tetraethylorthosilicate (TEOS, 99%) and $Ru(bipy)_3Cl_2{\cdot}6H_2O$ were purchased from Sigma-Aldrich, and 3-chloropropyltriethoxysilane (CPTS, >97%) was from TCI. 4,4′-Bipyridine (98%) was obtained from Energy Chemical (China), and sodium iodide (AR) was from Aladdin (China). Iodomethane was acquired from Xiya reagent (China), and doxorubicin hydrochloride (DOX) was from Meilun Biology Co. (Dalian, China). The other reagents used in these experiments were purchased from Nanjing Chemical Reagent Co. (China). All of the chemicals used were of analytical grade, and double-distilled water was used.

Instruments and Measurements. The small-angle powder X-ray diffraction (XRD) patterns of the MSN materials were measured on a Thermo ARL SCINTAG X'TRA diffractometer using a Cu Kα radiation (λ = 0.15405 nm), and the corresponding nitrogen adsorption−desorption isotherms were measured on an ASAP2020 porosimeter at 77 K for the determination of surface areas, cumulative pore volumes, and pore size distributions. The scanning electron microscope (SEM) and transmission electron microscope (TEM) images of the MSN materials were acquired on a Hitachi S-4800 microscope and on a JEM-2100 microscope, respectively. Thermogravimetric analysis (TGA) measurements were carried out on a TGA/SDT2960 thermogravimetric analyzer, using an oxidant atmosphere (air, 80 mL/min) with a heating program consisting on a heating ramp of 10 °C per minute from room temperature to 1000 °C. The solid-state ^{13}C NMR spectra were performed on a Bruker AVANCE400 NMR spectrometer at 400 MHz with 4 mm sample rotors in a triple resonance probe head. Zeta potentials were measured using a Zeta potential analyzer (Zetasizer Nano Z, Malvern Instruments Corp.). FTIR spectra were recorded on a VECTORTM22 spectrometer, and the time-dependent UV−vis spectra for cargo release were recorded using UV−vis spectroscopy on a Shimadzu UV-3600 spectrophotometer. 3-(4,5-Dimethylthiazol-2-yl)-2,5-diphenyltetrazolium bromide (MTT) assays were carried out on a BioTek-Instrument.

Synthesis of MCM-41. An aqueous solution of NaOH (2.0 M, 3.5 mL) was added to 480 mL of double-distilled water containing CTAB surfactants (1.0 g). The temperature of the solution was adjusted to 80 °C, and then, 5 mL of TEOS was added dropwise under vigorous stirring. After the reaction proceeded for 2 h, the white precipitates were collected by filtration, washed thoroughly with methanol and water, and dried at 70 °C overnight. To remove the CTAB templates, 1.6 g of the white precipitates was dispersed in 160 mL of methanol, and then, 9.0 mL of concentrated HCl solution was added. The solution mixture was heated to reflux for 24 h. The resulting product, i.e., MCM-41, was centrifugated, washed copiously with methanol, and dried in vacuum.

Preparation of BP-Functionalized MSNs (BP-MSNs). BP-PTS (0.4 mmol, 252 mg) was added to 20 mL of methanol containing MCM-41 (200 mg). The solution mixture was stirred at 40 °C under nitrogen atmosphere for 24 h. The product was centrifugated, washed with methanol, and dried in vacuum.

Preparation of DMBI-Functionalized MSNs (DMBI-MSNs). Synthetic iodopropyltriethoxysilane (IPTS, 1.32 mL) was added to 20 mL of dry toluene containing MCM-41 (660 mg). The solution mixture was stirred at 110 °C under nitrogen atmosphere for 24 h. The solid was recovered by centrifugation and washed by dry acetone followed by dispersing in 20 mL of dry acetone. After 2-mercaptobenzimidazole (1 g) and ethyldiisopropylamine (1 mL) was added, the mixture was refluxed under nitrogen atmosphere for 24 h followed by centrifugation, and the solid was washed thoroughly with acetone followed by redispersing in 10 mL of acetone. Excess iodomethane and ethyldiisopropylamine was added. The mixture was stirred at room temperature for 12 h and then refluxed for another 12 h. The final product was collected by centrifugation, washed successively with methanol, water, and methanol, and finally dried in vacuum.

Preparation of Cargo-Loaded, CPA[6]-Capped MSNs. A total of 250 mg of BP-MSNs or DMBI-MSNs was stirred in an aqueous solution of $Ru(bipy)_3Cl_2$ (4 mM, 50 mL) for 5 h. An excess of CPA[6] was added to the mixture, and then, the pH of the solution mixture was adjusted to be neutral. The resulting mixture was stirred for 24 h at room temperature. The cargo-loaded, CPA[6]-capped MSNs were collected by centrifugation and washed thoroughly with fresh double-distilled water.

Cargo Release. A desired amount of the cargo-loaded, CPA[6]-capped MSNs was placed in the bottom of a cuvette, and double-distilled water was added slowly in order not to interfere with the solid samples. The upper solution was stirred carefully with a plastic stick at intervals to facilitate the diffusion of released cargo, and the UV−vis absorption spectrum of the upper solution was recorded as a function of time. To trigger the release of cargo, the desired amounts of acids or competitive binding agents were added. Release efficiencies were calculated from the absorption maximum of $Ru(bipy)_3^{2+}$ at 453 nm. To assess the cargo release trigged by metal chelating, the neutral aqueous solutions of different divalent metal salts (1 mM, pH 7.0)

were prepared and then added to the cuvette instead of double-distilled water in the initial stage.

DOX Loading and Release. DMBI-MSNs (20 mg) were stirred in an aqueous solution of DOX (1 mM, 3 mL) at pH 7.0 overnight. An excess of CPA[6] was added to the mixture, and then, the pH of the solution mixture was adjusted to be neutral. The resulting mixture was stirred for 24 h at room temperature. The DOX-loaded, CPA[6]-capped MSNs were collected by centrifugation and washed thoroughly with fresh double-distilled water. To investigate the pH-responsive DOX release, the DOX-loaded, CPA[6]-capped MSNs were prepared in 5 mL of aqueous solution at different pH values in a dialysis bag, and the sealed dialysis bag was then submerged in 15 mL of water at the corresponding pH. The aqueous solutions containing the released DOX were collected at different time intervals for spectral analysis and replaced with an equal volume of water at the corresponding pH. The amounts of released DOX in the aqueous solutions were monitored using UV−vis spectroscopy with the absorption maximum of DOX at 497 nm.

MTT Assay. A549 cells were used to test the cytotoxicity of the CPA[6]-capped DMBI-MSNs with and without DOX loading. The cells were seeded in a 96-well plate at a density of 8000 cells/well for 24 h, and then, the CPA[6]-capped DMBI-MSNs with and without DOX loading were added with different concentrations of 0.25, 0.5, 1.0, 2.0, 4.0, 8.0, 16.0, 32.0, and 64.0 μg/mL. After 48 h of incubation, the media were removed, and the cells were continuously incubated in a medium containing 0.5 mg/mL MTT reagent for 4 h. Afterward, the crystallized formazan violet was redissolved in 150 μL of dimethyl sulfoxide at 37 °C. The absorbance at 490 nm was measured by a multidetection microplate reader.

RESULTS AND DISCUSSION

Construction of CPA[6]-Valved MSN Vehicles. MCM-41 nanoparticles were synthesized by the base-catalyzed sol−gel method. Both TEM and SEM images of MCM-41 (Supporting Information, Figure S19) showed that MSNs had roughly spherical shapes with an average diameter of about 110 nm. From the TEM image, it is clear that hexagonal-arrayed cylindrical nanopores were arranged parallel to each other, which was further confirmed by small-angle powder XRD patterns of MCM-41 with four well-resolved reflections indexed as (100), (110), (200), and (210) (Supporting Information, Figure S20), characteristic of two-dimensional hexagonal arrays of cylindrical pores.[36] Nitrogen adsorption−desorption isotherms of MCM-41 showed a typical curve of type IV with a surface area of 1013 m^2/g and an average pore size of 2.6 nm (Supporting Information, Figure S21).

CPA[6] and BP-PTS were synthesized and characterized with ^{1}H NMR and ^{13}C NMR spectra for confirmation of their chemical structures (Supporting Information, Figures S7, S8, S15, and S16). FTIR spectroscopy was used to characterize the modification of BP-PTS on the MSN surface (Supporting Information, Figure S22); the two peaks at 1639 and 1461 cm^{-1} were present, primarily owing to the C═N and C═C stretching vibrations of BP,[37] respectively. At the same time, the intensity of the band at 955 cm^{-1} related to silanols was reduced to some degree. After subsequent capping of CPA[6], a peak at 1504 cm^{-1} due to the skeletal stretching vibrations of phenyl rings appeared; moreover, a shoulder overlapped with the band at 1639 cm^{-1} and a peak at 1401 cm^{-1} were assigned to the antisymmetric and symmetric stretching vibrations of carboxylate groups of CPA[6], respectively.

Solid-state ^{13}C NMR spectroscopy was used to further characterize the modification of the BP-PTS and subsequent capping of CPA[6] (Figure 1). The resonances at 149.2, 146.1, and 127.2 ppm indicated the functionalization of BP. The appearance of the peak at 175.3 ppm, due to the ^{13}C resonance

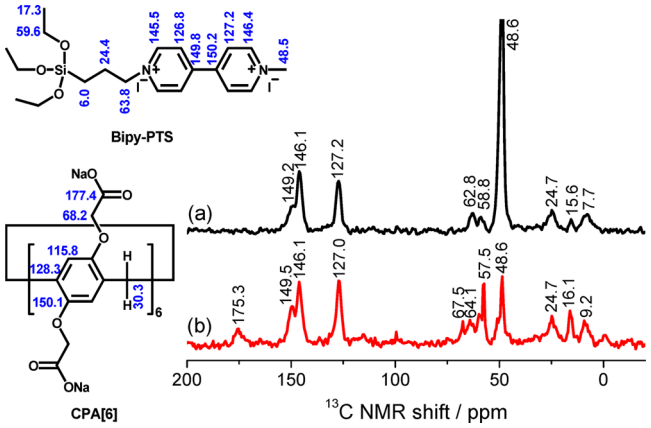

Figure 1. Solid-state ^{13}C NMR spectra of (a) BP-MSNs and (b) CPA[6]-capped BP-MSNs without cargo loading. The resonance at 48.6 ppm mostly resulted from the residual solvent methanol as well as methyl groups. The resonances labeled in the chemical structures of synthetic BP-PTS and CPA[6] come from their solution ^{13}C NMR spectra in D_2O (Supporting Information, Figures S8 and S16).

of the carboxylate groups, confirmed the threading of CPA[6] through the BP stalks for the development of supramolecular nanovalves.

The surface density of the BP functionalities was determined using TGA to be 0.21 mmol/g MSNs on the basis of the change of weight loss (Supporting Information, Figure S23). Upon threading of CPA[6] through the BP stalks on the MSN surface (without cargo loading), the capping amount of CPA[6] was also determined using TGA to be 54.6 mg/g BP-MSN (Supporting Information, Figure S23). The zeta potential of MCM-41 was −47.7 mV and increased to 58.6 mV upon immobilization of the BP stalks on the MSN surface and then decreased to −40.8 mV upon capping of CPA[6] (Supporting Information, Table S1). These results indicate that the constructed CPA[6]-capped BP-MSNs were highly negatively-charged and could be well dispersed in water.

In comparison to MCM-41, the TEM image of BP-MSNs remained almost unchanged, but the CPA[6]-capped BP-MSNs with the loading of $Ru(bipy)_3^{2+}$ did not show clear nanopore channels (Supporting Information, Figure S24). Energy dispersive spectroscopy (EDS) analysis from the corresponding SEM mode shows that the Ru elements were clearly detected after loading of $Ru(bipy)_3^{2+}$ (Supporting Information, Figure S25). BP-MSNs basically maintained the similar XRD patterns to MCM-41 although the weak reflection (210) nearly vanished (Supporting Information, Figure S26), which indicates that the mesoporous structure of silica matrix remained almost unchanged upon functionalization of BP, but only one reflection (100) with reduced intensity could be observed for the cargo-loaded, CPA[6]-capped BP-MSNs. The surface area of BP-MSNs decreased to 836 m^2/g, and the average pore size was 2.3 nm (Supporting Information, Figure S27 and Table S2). The surface area of the cargo-loaded, CPA[6]-capped BP-MSNs abruptly reduced to 39 m^2/g because the MSN pores were filled and capped (Supporting Information, Figure S27 and Table S2). Considering the dimensions of CPA[6] (ca. 1.51 nm in external diameter) and $Ru(bipy)_3^{2+}$ (sphere-like shape, ca. 1.46 nm in diameter) (Supporting Information, Figure S28), $Ru(bipy)_3^{2+}$ could be entrapped in the BP-MSN pores (2.3 nm) followed by tight capping with two adjacent CPA[6] nanovalves. These results indicate that the cargo-

loaded, CPA[6]-capped BP-MSN vehicles were constructed. The loading capacity of $Ru(bipy)_3^{2+}$ after CPA[6] capping was determined using UV−vis spectroscopy to be 0.358 mmol/g BP-MSNs, much higher than the adsorbed amount of 0.028 mmol/g without CPA[6] capping after washing, which indicates that the CPA[6] nanovalves played an important role in cargo loading and subsequent controlled release.

DMBI-SM was synthesized and characterized with ^{1}H NMR and ^{13}C NMR spectra for structural confirmation (Supporting Information, Figures S9 and S10). All of the proton resonances of DMBI-SM shifted upfield dramatically upon addition of 1 equiv of CPA[6] due to the shielding effect of the electron-rich cavity of CPA[6] (Figure 2), which indicates that DMBI-SM

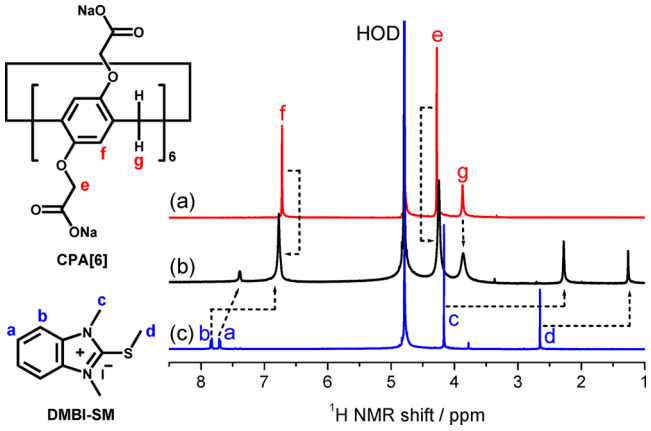

Figure 2. ^{1}H NMR spectra of (a) 3 mM CPA[6], (b) 3 mM CPA[6] and 3 mM DMBI-SM, and (c) 3 mM DMBI-SM in D_2O.

was completely encapsulated inside the CPA[6] cavity. Further ^{1}H NMR titration studies indicate that DMBI-SM and CPA[6] could form a stable 1:1 binding stoichiometry with a high association constant of $(2.82 \pm 1.83) \times 10^5$ M^{-1} (Supporting Information, Figures S29 and S30). After MSNs were finally functionalized with DMBI moieties (DMBI-MSNs), a peak at 1482 cm^{-1} was observed due to the in-phase scissoring vibration of methyl groups of DMBI[38] as well as the skeletal stretching vibrations (1448 cm^{-1})[38] and out-of-plane C−H wagging modes (750 cm^{-1})[38] of DMBI aryl rings (Supporting Information, Figure S31A). After subsequent capping of CPA[6], a peak at 1500 cm^{-1} was clearly observed, due to the skeletal stretching vibrations of CPA[6] phenyl rings (Supporting Information, Figure S31B). The corresponding solid-state ^{13}C NMR spectrum shows a group of resonances in the range of 152−112 ppm relevant to the benzimidazole functionalities and a resonance at 32.6 ppm relevant to the methylation of the benzimidazole functionalities (Supporting Information, Figure S32), which confirm that the MSN surface was functionalized with the DMBI moieties. The zeta potential was increased from −47.7 to 14.0 mV upon functionalization of DMBI stalks on the MSN surface and then decreased to −35.9 mV upon encircling of CPA[6] (Supporting Information, Table S3). It is obvious that the CPA[6]-capped DMBI-MSNs were highly negative-charged and could be well dispersed in water. DMBI-MSNs showed the similar XRD patterns to BP-MSNs, but a very weak reflection peak could only be observed after loading of $Ru(bipy)_3^{2+}$ and capping of CPA[6] (Supporting Information, Figure S33). The surface area of DMBI-MSNs decreased to 822 m^2/g, and the average pore size was 2.1 nm (Supporting Information, Figure S34 and Table S4). The surface area of the cargo-loaded, CPA[6]-capped DMBI-MSNs steeply reduced to 167 m^2/g because the MSN pores were filled and capped (Supporting Information, Figure S34 and Table S4). These results indicate that the cargo-loaded, CPA[6]-capped DMBI-MSN vehicles were constructed. The loading capacities of $Ru(bipy)_3^{2+}$, after DMBI-MSNs were capped with and without CPA[6], were determined to be 0.301 and 0.053 mmol/g DMBI-MSN, respectively, using UV−vis spectroscopy, which indicates the role of the CPA[6] nanovalves in cargo loading and subsequent controlled release.

pH-Triggered Controlled Release. UV−vis spectroscopy was used to monitor release of $Ru(bipy)_3^{2+}$ from the CPA[6]-capped MSNs functionalized with the BP or DMBI stalks (Supporting Information, Figures S35 and S36). Prior to pH trigger, both of the systems showed minimal premature release of cargo of less than 9% after 5 h (Figure 3). Upon lowering of

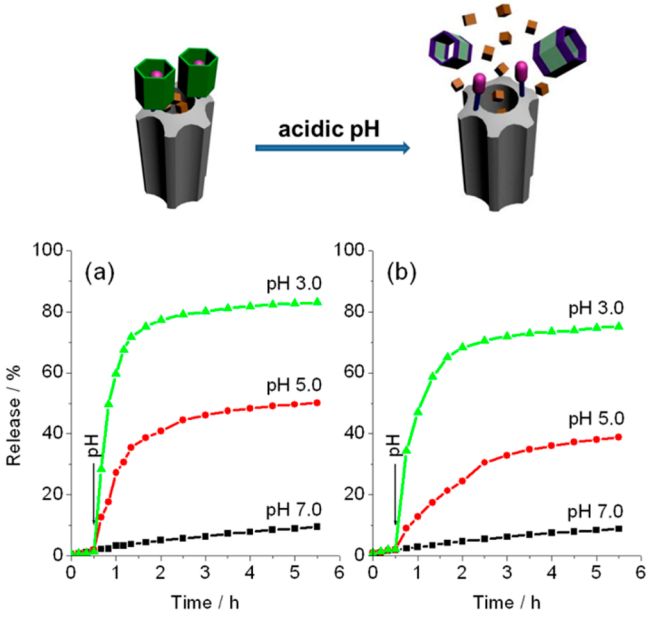

Figure 3. pH-responsive release profiles of $Ru(bipy)_3^{2+}$ from (a) CPA[6]-valved BP-MSNs and (b) CPA[6]-valved DMBI-MSNs. The arrow indicates the change of pH.

the pH, the carboxylate groups of CPA[6] were protonated to become carboxylic acids, resulting in the decrease of negative charges and solubility of CPA[6].[32] These changes caused the weakening of the electrostatic interactions between CPA[6] and the BP/DMBI stalks[32] and the dethreading of CPA[6] from the stalks, leading to the opening of the nanovalves and the release of entrapped cargo. The release efficiencies increased with a decrease in pH but were different, to some degree, for the two systems. After the cargo was released from the CPA[6]-capped BP-MSNs at pH 3.0, the MSN pore channels could be clearly observed from the TEM image similar to those of BP-MSNs (Supporting Information, Figure S24). The integrity and mesoporous structures of MSNs remained almost unchanged after cargo release under acidic conditions. The intensities of the XRD peaks were restored to a great degree but were still weaker than those of BP-MSNs (Supporting Information, Figure S26), and the surface area rebounded to 693 m^2/g from 30 m^2/g along with a recovery of the nanopores to the average size of 2.0 nm (Supporting Information, Figure S27 and Table S2). The incomplete

dx.doi.org/10.1021/am506004q | ACS Appl. Mater. Interfaces 2014, 6, 20430−20436

recovery of these parameters might be ascribed to the release efficiency of 83%. Similarly, after the cargo was released from the CPA[6]-capped DMBI-MSNs at pH 3.0, the XRD peaks, surface area, and pore size were restored to a great degree (Supporting Information, Figures S33 and S34 and Table S4).

Metal Chelating-Triggered Controlled Release. It is known that carboxylate groups can bind with divalent metal ions and their binding affinity follows the order $Cu^{2+} > Zn^{2+} > Ni^{2+} > Ca^{2+} \approx Mg^{2+}$ for 1:1 complexes, which is 1−3 orders of magnitude smaller than the pK_a (3.12 at 25 °C) of phenoxyacetic acid.[39] CPA[6] is cylindrical-shaped with 6 carboxylate groups at each end. In the presence of divalent metal ions, the carboxylate groups of CPA[6] were chelated by the metal ions, which resulted in the decrease of the negative charges of CPA[6] and the weakening of the binding affinity of CPA[6] for the BP or DMBI stalks, so that the CPA[6] nanovalves were opened and the cargo was released from the MSN pores with different efficiencies for the two systems (Figure 4 and Supporting Information, Figures S37 and S38).

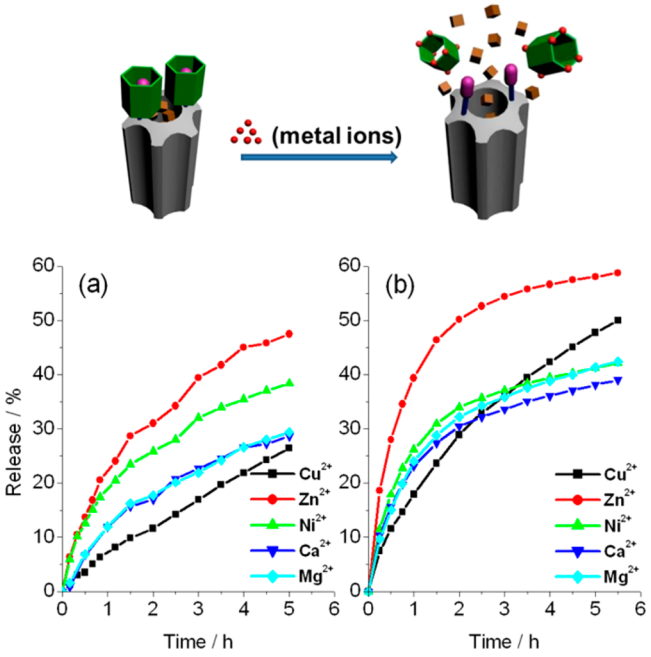

Figure 4. Release profiles of $Ru(bipy)_3^{2+}$ from (a) CPA[6]-valved BP-MSNs and (b) CPA[6]-valved DMBI-MSNs by metal chelating of different divalent metal ions (1 mM) at pH 7.0.

The metal chelating-triggered release was carried out at neutral pH to avoid the interference from acidic pH. Except for Cu^{2+}, the release efficiencies triggered by other metal ions followed the order of the binding affinity of the metal ion−carboxylate complexes (1:1). The abnormal release behavior in the case of Cu^{2+} could be ascribed to the relatively high side reaction coefficient of Cu^{2+} at neutral pH (i.e., $Cu(OH)_2$ species of low solubility were readily formed) and the coordination equilibrium between the Cu states.

Competitive Binding-Triggered Controlled Release. The controlled release of the two systems was further investigated by competitive binding of MV, leading to the continuous dethreading of CPA[6] from the BP or DMBI stalks, the opening of the nanovalves, and the release of cargo from the MSN pores (Figure 5 and Supporting Information, Figures S39 and S40). The release efficiencies increased with

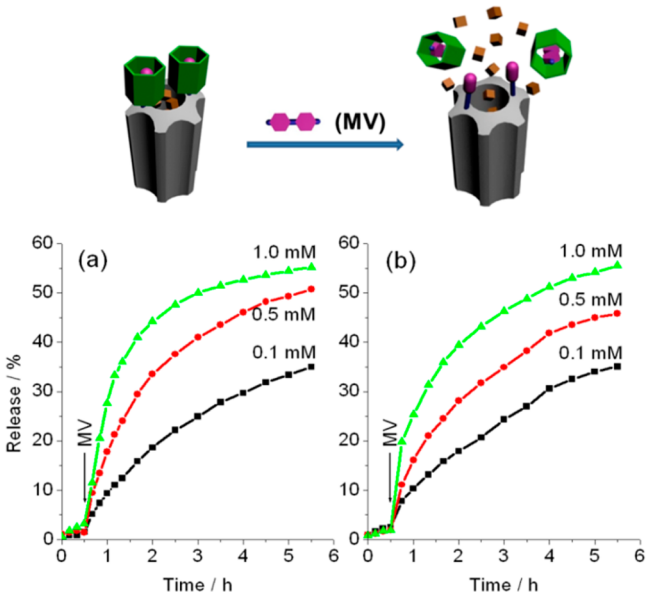

Figure 5. Release profiles of $Ru(bipy)_3^{2+}$ from (a) CPA[6]-valved BP-MSNs and (b) CPA[6]-valved DMBI-MSNs by competitive binding of MV at pH 7.0. The arrow indicates the addition of MV.

the increase of MV concentration and were almost identical for the two systems. It is clear that the release efficiency was related to the nature and surface density of functionalized stalks and the loading capacity of cargo as well as the binding affinity of CPA[6] for the stalks.

Drug Release, Cytotoxicity, and Antitumor Efficiency. The antitumor drug DOX (ca. 1.64 × 1.22 nm) (Supporting Information, Figure S28) was used to investigate drug release from the CPA[6]-valved DMBI-MSN vehicles for potential biological applications. The pH-responsive controlled release of DOX from the CPA[6]-valved DMBI-MSNs was investigated (Figure 6a). The loading capacity of DOX was determined to be 0.134 mmol/g DMBI-MSN using UV−vis spectroscopy. A significant release of DOX was observed at pH 5.0 in comparison to the case at pH 7.0. Furthermore, the in vitro cytotoxicity and antitumor efficiency of the CPA[6]-valved DMBI-MSNs with and without loading of DOX were evaluated by the MTT assay after 48 h of incubation with A549 cells (Figure 6b). The CPA[6]-valved MSNs without drug loading showed a low cytotoxicity; however, the CPA[6]-valved MSNs with DOX loading showed antiproliferative activity with a cell viability of about 20%. It is well documented that the pH in tumor and inflammatory tissues is more acidic than in blood and normal tissues, with early endosomes and late endosomes/lysosomes in the intracellular environments of tumor cells around pH 6.0 and 5.0, respectively.[40] Zinc is one kind of important trace element in the human body, and its content in blood is relatively low (about 0.014−0.015 mM in serum and plasma and 0.15−0.2 mM in red blood cells). It is likely that the premature release of drugs from the CPA[6]-valved MSNs under physiological conditions can almost be avoided. When the drug-loaded, CPA[6]-valved DMBI-MSNs are delivered to target tumor cells and internalized by the tumor cells, pH-triggered drug release from the CPA[6]-valved MSNs may be a major pathway in the intracellular environments around pH 5.0, while Zn^{2+}-triggered drug release would be inhibited to some degree at pH 5.0. These results indicate that the constructed

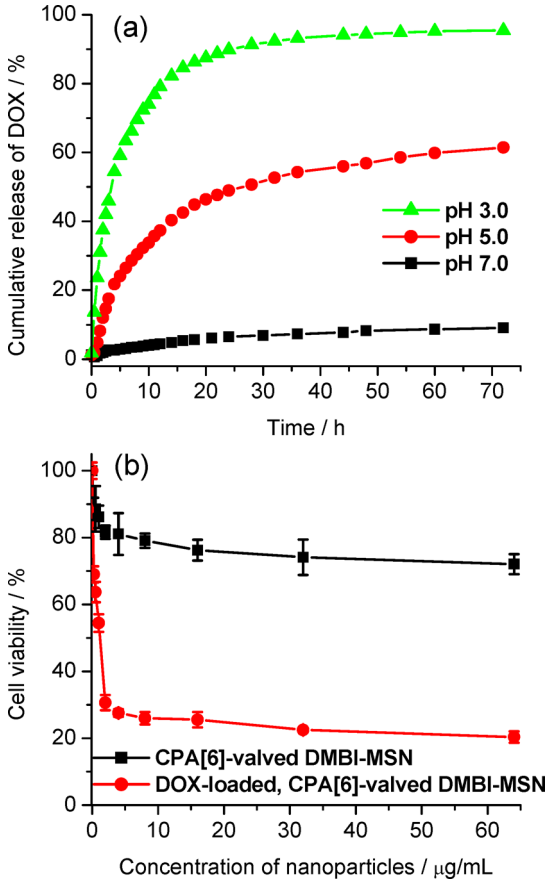

Figure 6. (a) pH-triggered release profiles of DOX from CPA[6]-valved DMBI-MSNs at different pH values. (b) Cell viability of CPA[6]-valved DMBI-MSNs with and without loading of DOX after 48 h of incubation with A549 cells.

CPA[6]-valved MSN delivery systems have promising biological applications in targeted drug therapy.

CONCLUSIONS

In summary, the new guest DMBI-SM was synthesized to form a 1:1 inclusion complex with CPA[6] with a high binding affinity, and the two systems of CPA[6]-valved MSNs functionalized with the BP or DMBI stalks were constructed for multiresponsive controlled release. The release of cargo could be triggered by three pathways, including acidic pH, metal chelating, and competitive binding, to activate the nanovalves for the dethreading of CPA[6] from the BP or DMBI stalks. Coordination chemistry is the first strategy for the activation of CPA nanovalves in MSN-based delivery systems. The controlled release of the CPA[6]-valved MSN systems can meet diverse requirements and has promising applications in targeted drug therapy.

ASSOCIATED CONTENT

Supporting Information

Synthesis details and ^{1}H and ^{13}C NMR characterizations, TEM and SEM images, XRD, nitrogen adsorption−desorption isotherms and pore size distributions, TGA, zeta potentials, ^{1}H NMR, ^{13}C NMR, FTIR, and UV−vis spectra. This material is available free of charge via the Internet at http://pubs.acs.org.

AUTHOR INFORMATION

Corresponding Author

*E-mail: xzdu@nju.edu.cn.

Notes

The authors declare no competing financial interest.

ACKNOWLEDGMENTS

This work was supported by National Natural Science Foundation of China (21273112) and Natural Science Foundation of Jiangsu Province (BK2012719). We thank Dr. Xiaokang Ke at the School of Chemistry and Chemical Engineering of Nanjing University for his contribution of the 400 MHz solid-state NMR spectra.

REFERENCES

(1) Slowing, I. I.; Vivero-Escoto, J. L.; Wu, C.-W.; Lin, V. S.-Y. Mesoporous Silica Nanoparticles as Controlled Release Drug Delivery and Gene Transfection Carriers. *Adv. Drug Delivery Rev.* **2008**, *60*, 1278−1288.

(2) Coti, K. K.; Belowich, M. E.; Liong, M.; Ambrogio, M. W.; Lau, Y. A.; Khatib, H. A.; Zink, J. I.; Khashab, N. M.; Stoddart, J. F. Mechanised Nanoparticles for Drug Delivery. *Nanoscale* **2009**, *1*, 16−39.

(3) Popat, A.; Hartono, S. B.; Stahr, F.; Liu, J.; Qiao, S. Z.; Lu, G. Q. Mesoporous Silica Nanoparticles for Bioadsorption, Enzyme Immobilisation, and Delivery Carriers. *Nanoscale* **2011**, *3*, 2801−2818.

(4) Yang, Y.-W.; Sun, Y.-L.; Song, N. Switchable Host-Guest Systems on Surfaces. *Acc. Chem. Res.* **2014**, *47*, 1950−1960.

(5) Yang, P. P.; Gai, S. L.; Lin, J. Functionalized Mesoporous Silica Materials for Controlled Drug Delivery. *Chem. Soc. Rev.* **2012**, *41*, 3679−3698.

(6) Coll, C.; Bernardos, A.; Martínez-Máñez, R.; Sancenón, F. Gated Silica Mesoporous Supports for Controlled Release and Signaling Applications. *Acc. Chem. Res.* **2013**, *46*, 339−349.

(7) Nguyen, T. D.; Liu, Y.; Saha, S.; Leung, K. C. F.; Stoddart, J. F.; Zink, J. I. Design and Optimization of Molecular Nanovalves Based on Redox-Switchable Bistable Rotaxanes. *J. Am. Chem. Soc.* **2007**, *129*, 626−634.

(8) Park, C.; Oh, K.; Lee, S. C.; Kim, C. Controlled Release of Guest Molecules from Mesoporous Silica Particles Based on a pH-Responsive Polypseudorotaxane Motif. *Angew. Chem., Int. Ed.* **2007**, *46*, 1455−1457.

(9) Patel, K.; Angelos, S.; Dichtel, W. R.; Coskun, A.; Yang, Y. W.; Zink, J. I.; Stoddart, J. F. Enzyme-Responsive Snap-Top Covered Silica Nanocontainers. *J. Am. Chem. Soc.* **2008**, *130*, 2382−2383.

(10) Ferris, D. P.; Zhao, Y. L.; Khashab, N. M.; Khatib, H. A.; Stoddart, J. F.; Zink, J. I. Light-Operated Mechanized Nanoparticles. *J. Am. Chem. Soc.* **2009**, *131*, 1686−1688.

(11) Park, C.; Kim, H.; Kim, S.; Kim, C. Enzyme Responsive Nanocontainers with Cyclodextrin Gatekeepers and Synergistic Effects in Release of Guests. *J. Am. Chem. Soc.* **2009**, *131*, 16614−16615.

(12) Park, C.; Lee, K.; Kim, C. Photoresponsive Cyclodextrin-Covered Nanocontainers and Their Sol-Gel Transition Induced by Molecular Recognition. *Angew. Chem., Int. Ed.* **2009**, *48*, 1275−1278.

(13) Wang, C.; Li, Z. X.; Cao, D.; Zhao, Y. L.; Gaines, J. W.; Bozdemir, O. A.; Ambrogio, M. W.; Frasconi, M.; Botros, Y. Y.; Zink, J. I.; Stoddart, J. F. Stimulated Release of Size-Selected Cargos in Succession from Mesoporous Silica Nanoparticles. *Angew. Chem., Int. Ed.* **2012**, *51*, 5460−5465.

(14) Sun, Y. L.; Zhou, Y.; Li, Q. L.; Yang, Y. W. Enzyme-Responsive Supramolecular Nanovalves Crafted by Mesoporous Silica Nanoparticles and Choline-Sulfonatocalix[4]arene [2]Pseudorotaxanes for Controlled Cargo Release. *Chem. Commun.* **2013**, *49*, 9033−9035.

(15) Li, H.; Tan, L.-L.; Jia, P.; Li, Q.-L.; Sun, Y.-L.; Zhang, J.; Ning, Y.-Q.; Yu, J.; Yang, Y.-W. Near-Infrared Light-Responsive Supramolecular Nanovalve Based on Mesoporous Silica-Coated Gold Nanorods. *Chem. Sci.* **2014**, *5*, 2804−2808.

(16) Angelos, S.; Yang, Y. W.; Patel, K.; Stoddart, J. F.; Zink, J. I. pH-Responsive Supramolecular Nanovalves Based on Cucurbit[6]uril Pseudorotaxanes. *Angew. Chem., Int. Ed.* **2008**, *47*, 2222−2226.
(17) Angelos, S.; Khashab, N. M.; Yang, Y. W.; Trabolsi, A.; Khatib, H. A.; Stoddart, J. F.; Zink, J. I. pH Clock-Operated Mechanized Nanoparticles. *J. Am. Chem. Soc.* **2009**, *131*, 12912−12914.
(18) Angelos, S.; Yang, Y. W.; Khashab, N. M.; Stoddart, J. F.; Zink, J. I. Dual-Controlled Nanoparticles Exhibiting AND Logic. *J. Am. Chem. Soc.* **2009**, *131*, 11344−11346.
(19) Khashab, N. M.; Trabolsi, A.; Lau, Y. A.; Ambrogio, M. W.; Friedman, D. C.; Khatib, H. A.; Zink, J. I.; Stoddart, J. F. Redox- and pH-Controlled Mechanized Nanoparticles. *Eur. J. Org. Chem.* **2009**, 1669−1673.
(20) Liu, J.; Du, X. pH- and Competitor-Driven Nanovalves of Cucurbit[7]uril Pseudorotaxanes Based on Mesoporous Silica Supports for Controlled Release. *J. Mater. Chem.* **2010**, *20*, 3642−3649.
(21) Liu, J.; Du, X.; Zhang, X. Enzyme-Inspired Controlled Release of Cucurbit[7]uril Nanovalves by Using Magnetic Mesoporous Silica. *Chem.—Eur. J.* **2011**, *17*, 810−815.
(22) Sun, Y. L.; Yang, B. J.; Zhang, S. X. A.; Yang, Y. W. Cucurbit[7]uril Pseudorotaxane-Based Photoresponsive Supramolecular Nanovalve. *Chem.—Eur. J.* **2012**, *18*, 9212−9216.
(23) Chen, T.; Yang, N.; Fu, J. Controlled Release of Cargo Molecules from Hollow Mesoporous Silica Nanoparticles Based on Acid and Base Dual-Responsive Cucurbit[7]uril Pseudorotaxanes. *Chem. Commun.* **2013**, *49*, 6555−6557.
(24) Wang, M.; Chen, T.; Ding, C.; Fu, J. Mechanized Silica Nanoparticles Based on Reversible Bistable [2]Pseudorotaxanes as Supramolecular Nanovalves for Multistage pH-Controlled Release. *Chem. Commun.* **2014**, *50*, 5068−5071.
(25) Ogoshi, T.; Kanai, S.; Fujinami, S.; Yamagishi, T. A.; Nakamoto, Y. para-Bridged Symmetrical Pillar[5]arenes: Their Lewis Acid Catalyzed Synthesis and Host-Guest Property. *J. Am. Chem. Soc.* **2008**, *130*, 5022−5023.
(26) Xue, M.; Yang, Y.; Chi, X.; Zhang, Z.; Huang, F. Pillararenes, a New Class of Macrocycles for Supramolecular Chemistry. *Acc. Chem. Res.* **2012**, *45*, 1294−1308.
(27) Zhang, H. C.; Zhao, Y. L. Pillararene-Based Assemblies: Design Principle, Preparation and Applications. *Chem.—Eur. J.* **2013**, *19*, 16862−16879.
(28) Ogoshi, T.; Kida, K.; Yamagishi, T. Photoreversible Switching of the Lower Critical Solution Temperature in a Photoresponsive Host-Guest System of Pillar[6]arene with Triethylene Oxide Substituents and an Azobenzene Derivative. *J. Am. Chem. Soc.* **2012**, *134*, 20146−20150.
(29) Li, C.; Ma, J.; Zhao, L.; Zhang, Y.; Yu, Y.; Shu, X.; Lia, J.; Jia, X. Molecular Selective Binding of Basic Amino Acids by a Water-Soluble Pillar[5]arene. *Chem. Commun.* **2013**, *49*, 1924−1926.
(30) Chen, W.; Zhang, Y.; Li, J.; Lou, X.; Yu, Y.; Jia, X.; Li, C. Synthesis of a Cationic Water-Soluble Pillar[6]arene and Its Effective Complexation Towards Naphthalenesulfonate Guests. *Chem. Commun.* **2013**, *49*, 7956−7958.
(31) Sun, Y. L.; Yang, Y. W.; Chen, D. X.; Wang, G.; Zhou, Y.; Wang, C. Y.; Stoddart, J. F. Mechanized Silica Nanoparticles Based on Pillar[5]arenes for on-Command Cargo Release. *Small* **2013**, *9*, 3224−3229.
(32) Yu, G.; Xue, M.; Zhang, Z.; Li, J.; Han, C.; Huang, F. A Water-Soluble Pillar[6]arene: Synthesis, Host-Guest Chemistry, and Its Application in Dispersion of Multiwalled Carbon Nanotubes in Water. *J. Am. Chem. Soc.* **2012**, *134*, 13248−13251.
(33) Yu, G.; Zhou, X.; Zhang, Z.; Han, C.; Mao, Z.; Gao, C.; Huang, F. Pillar[6]arene/Paraquat Molecular Recognition in Water: High Binding Strength, pH-Responsiveness, and Application in Controllable Self-Assembly, Controlled Release, and Treatment of Paraquat Poisoning. *J. Am. Chem. Soc.* **2012**, *134*, 19489−19497.
(34) Duan, Q.; Cao, Y.; Li, Y.; Hu, X.; Xiao, T.; Lin, C.; Pan, Y.; Wang, L. pH-Responsive Supramolecular Vesicles Based on Water-Soluble Pillar[6]arene and Ferrocene Derivative for Drug Delivery. *J. Am. Chem. Soc.* **2013**, *135*, 10542−10549.
(35) Pescatori, L.; Arduini, A.; Pochini, A.; Secchi, A.; Massera, C.; Ugozzoli, F. Monotopic and Heteroditopic Calix[4]arene Receptors as Hosts for Pyridinium and Viologen Ion Pairs: A Solution and Solid-State Study. *Org. Biomol. Chem.* **2009**, *7*, 3698−3708.
(36) Kresge, C. T.; Leonowicz, M. E.; Roth, W. J.; Vartuli, J. C.; Beck, J. S. Ordered Mesoporous Molecular-Sieves Synthesized by a Liquid-Crystal Template Mechanism. *Nature* **1992**, *359*, 710−712.
(37) Bae, I. T.; Huang, H.; Yeager, E. B.; Scherson, D. A. In Situ Infrared Spectroscopic Studies of Redox Active Self-Assembled Monolayers on Gold Electrode Surfaces. *Langmuir* **1991**, *7*, 1558−1562.
(38) Malek, K.; Puc, A.; Schroeder, G.; Rybachenko, V. I.; Proniewicz, L. M. FT-IR and FT-Raman Spectroscopies and DFT Modelling of Benzimidazolium Salts. *Chem. Phys.* **2006**, *327*, 439−451.
(39) Bunting, J. W.; Thong, K. M. Stability Constants for Some 1:1 Metal-Carboxylate Complexes. *Can. J. Chem.* **1970**, *48*, 1654−1656.
(40) Miyata, K.; Oba, M.; Nakanishi, M.; Fukushima, S.; Yamasaki, Y.; Koyama, H.; Nishiyama, N.; Kataoka, K. Polyplexes from Poly(aspartamide) Bearing 1,2-Diaminoethane Side Chains Induce pH-Selective, Endosomal Membrane Destabilization with Amplified Transfection and Negligible Cytotoxicity. *J. Am. Chem. Soc.* **2008**, *130*, 16287−16294.